2020-01-01

An Accelerated Creep Testing Program For Nickel Based Superalloys

Robert M. Mach
University of Texas at El Paso

AN ACCELERATED CREEP TESTING PROGRAM FOR NICKEL BASED SUPERALLOYS

ROBERT MIGUEL MACH

Master's Program in Mechanical Engineering

APPROVED:

Calvin M. Stewart, Ph.D., Chair

Steve Stafford, Ph.D

Alejandra Castellanos, Ph.D

Stephen L. Crites, Jr., Ph.D.
Dean of the Graduate School

DEDICATION

Dedicated to my mom and dad, Adriana and John Mach.

AN ACCELERATED CREEP TESTING PROGRAM FOR NICKEL BASED SUPERALLOYS

by

ROBERT MACH, B.Sc.

THESIS

Presented to the Faculty of the Graduate School of

The University of Texas at El Paso

in Partial Fulfillment

of the Requirements

for the Degree of

MASTER OF SCIENCE

Department of Mechanical Engineering

THE UNIVERSITY OF TEXAS AT EL PASO

May 2020

ACKNOWLEDGEMENTS

I would like to thank my advisor Dr. Calvin Stewart for accepting to mentor me through my undergraduate degree and continuously pushing me through graduate school. I would also like to thank my colleagues, friends, and loved ones who have supported me in my undergraduate and graduate studies.

ABSTRACT

In order to improve the energy production within the United States, new materials are developed with the goal of increased functionality. These materials are required to perform at extreme pressures and temperatures (up to and beyond 200MPa and 650°C) as well as be sustainable beyond 10^5 hours. Before developing these materials into components for power generation, mechanical testing is required to better understand the behavior of these materials at various loads and temperatures. The longest of these tests is the conventional creep test which is a real time test that can beyond 10^5 hours depending on service conditions. Hundreds of specimens must be tested before being approved for use in power generation, but it is extremely difficult to rapidly qualify when each material is required to exceed 10^5 hours making testing through conventional means unfeasible. While others have designed accelerated testing methods to help qualify materials, many of these experiments use an empirical approach that requires test data to fit already existing creep data. In this study, an accelerated creep test called the stepped isostress method (SSM) is then applied to wrought Inconel 718 (IN 718) specimens. A test matrix is designed using deformation mechanism maps, time-temperature-transformation diagrams, and time-temperature-precipitation diagrams, in order to ensure that microstructurally, the accelerated creep tests fail similarly to the conventional creep tests. The data from the stepped isostress method is then applied to the McVetty and Sin-hyperbolic (Sinh) constitutive models in order to generate a creep master curve. The results from the model fits are then compared to the conventional creep data done from experiments as well as from the NIMS database for Inconel 718. Optical microscopy and scanning electron microscopy are used to compare the evolution of the microstructure from the conventional creep and accelerated creep tests. It is found that using the Sinh model on the accelerated creep data provides reasonable creep rupture predictions when

compared to the scatter band of creep tests. It was also observed that the microstructural evolution between the SSM experiments and creep tests were very similar in terms of the volume fraction of precipitates and phases.

TABLE OF CONTENTS

ACKNOWLEDGEMENTS v

ABSTRACT vi

TABLE OF CONTENTS vi

LIST OF TABLES x

LIST OF FIGURES xi

CHAPTER 1: INTRODUCTION 1

1.1 Motivation 1

1.2 Literature Review 2

1.3 Research Objectives 6

1.4 Organization 7

CHAPTER 2: MATERIALS AND EQUIPMENT 8

2.1 Material: Inconel 718 8

2.2 Equipment 11

CHAPTER 3: ACCELERATED CREEP TESTING 12

3.1 Experiments 12

3.2 CCT and SSM Results 15

3.3 Microstructural Comparison 17

CHAPTER 4: APPLICATION OF THE THETA PROJECTION MODEL TO ACT DATA 19

4.1 Theta Projection Model 19

4.2 Methodology 20

4.3 MATLAB Code 26

4.4 Results 27

CHAPTER 5: APPLICATION OF THE SINH MODEL TO THE SSM TESTS 29

5.1 Sinh Model 29

5.2 Methodology 30

5.3 Results 35

CHAPTER 6: CONCLUSIONS AND FUTURE WORK 37

6.1 Conclusions 37

6.2 Future Work 38
REFERENCES 40
VITA 44

LIST OF TABLES

Table 2.1: Chemical composition (wt%) of Inconel 718 [42] 9

Table 2.2: Monotonic tensile properties of IN 718 at 650°C 10

Table 3.1: Test matrix for CCT tests..... 12

Table 3.2: Test matrix for SSM tests 14

Table 3.3: Data for conventional creep testing of IN718 15

Table 3.4: Stepped Isostress Data of IN718 16

Table 4.1: Accelerated SSM Data at 650°C..... 28

Table 5.1: Analytically calibrated material constants of Sinh for triplicate SSM at 650°C..... 36

Table 5.2: Percentage of creep damage and instantaneous plastic damage in SSM at 650°C 36

LIST OF FIGURES

Figure 1.1– Creep deformation curve 2

Figure 1.2 – Schematic of small punch creep test [13] 3

Figure 1.3 – Ultrafast creep method [17] 3

Figure 1.4 - Time-Temperature-Stress Superposition Principle (TTSSP) visualization of (a) reference stress or temperature level (b) stress or temperature step (c) elevated stress or temperature level (d) accelerated creep strain 4

Figure 2.1 - Optical microscopy of Inconel 718 specimens 8

Figure 2.2 – Specimen dimensions for testing 9

Figure 2.3 – Stress-strain curves of IN 718 10

Figure 2.4 – Experimental setup for mechanical testing in Instron 5969 11

Figure 3.1 – Deformation Mechanism Map of Nickel 20%Chromium Alloy [45] 12

Figure 3.2 – Time-Temperature-Transformation Diagram of IN718 13

Figure 3.3 – Time-Temperature-Phase Diagram of IN718 13

Figure 3.4 – Results from CCT experiments on IN718 at 650℃ 15

Figure 3.5 – Results from SSM experiments on IN718 at 650℃ 16

Figure 3.6 – SEM backscatter image of conventional creep testing 17

Figure 3.7 – SEM backscatter image of stepped isostress method 17

Figure 4.1 – Depiction of how constitutive models are applied to accelerated creep data: (a) gathering of SSM results, (b) removal of elastic, plastic, thermal strains to ensure only creep strain, (c) location of the virtual start time at each step, (d) zeroing at each start time, (e) user applies a polynomial like what is done in literature to fit data and generate a master curve, (f)

application of constitutive model and calibrating material constants (g) generation of creep master curve.....20
Figure 4.2 - Illustration of time-shift sensitivity issues for (a) a narrow and (b) wide time overlap 25
Figure 4.3 - MATLAB Code Map for Theta Projection 26
Figure 4.4 – Comparison of Theta Projection with Conventional Creep Tests.....27
Figure 5.1 – An illustration of the calibration approach by Sinh model for SSM test data 30
Figure 5.2 - Calibrated (a) λ and (b) ϕ for triplicate SSM across multiple stress at 650°C.....34
Figure 5.3 - Comparison of Sinh extrapolated CCTs with experimental CCTs and SSMs 35

CHAPTER 1: INTRODUCTION

1.1 Motivation

With the development of ultra-supercritical (USC) power plants on the rise, the need for materials to survive extreme temperatures and pressures (up to 750℃ and 100 MPa for 200,000 hours) is required [1-[2]. At these extreme environments, components such as heat exchanger tubing, nuclear reactors and turbine blades are subjected to fatigue, creep, corrosion, and oxidation, which can greatly shorten the life of the materials. Creep rupture is an important factor that must be considered when designing materials for USC power plants [4]. Extensive research and development for these materials is required to determine their behavior in extreme environments. One method to determine creep behavior includes conducting creep tests to gather creep deformation, rupture, and minimum-creep-strain-rate data. The problem with this method lies with the time and money required to run these experiments. Another method scientist can use for studying creep behavior is via creep prediction models. Issues with this method is that it is reliant on existing creep data. In order to align with goals of generating operational USC power plants by 2030, accelerated testing must be done to ensure these materials are ready for service [3]. The focus of this study is to develop methodological and mathematical criterion for accelerated creep testing and prove whether accelerated creep testing is a viable supplement to conventional creep testing.

1.2 Literature Review

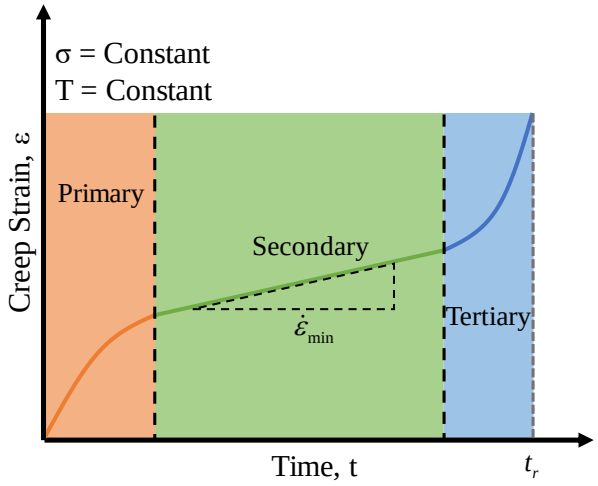

Figure 1.1– Creep deformation curve

Creep is a phenomenon that occurs when a material plastically deforms when subjected to a constant stress and temperature over a period of time. This deformation can occur well below the yield stress of a material but is even more prevalent at elevated temperatures [5[*6*]. Creep deformation is divided into three distinct stages: primary, secondary, and tertiary creep [5[*6*]. A typical conventional creep curve is depicted in Figure 1.*1*. In the primary creep stage, the creep strain rate is initially high but gradually decreases to a constant rate. In superalloys, that amount of deformation that occurs in primary creep is minimal when compared to the deformation that occurs within the other stages. The secondary creep stage or steady-state creep is the stage where strain hardening and recovery mechanics are in balance which cause strain. This behavior is known as the minimum-creep-strain-rate, $\dot{\varepsilon}_{min}$ [7]. Once a material reaches the tertiary creep stage, the strain increases exponentially until rupture, t_r.

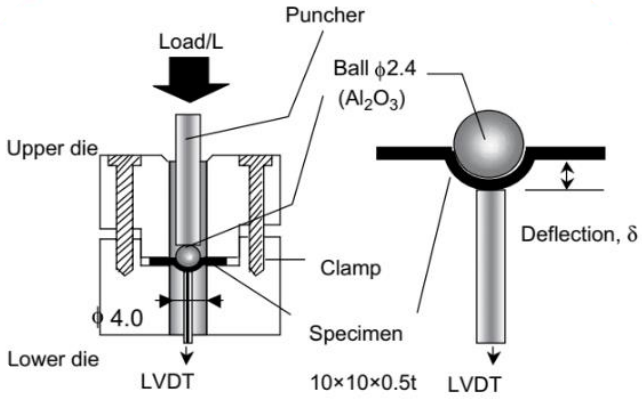

Figure 1.2 – Schematic of small punch creep test [14]

Accelerated creep testing (ACT) is the gathering of short-term physical data for predictions of long-term behavior [8]. While accelerated creep testing has been proven to be an effective method for predicting creep rupture in polymer and fibrous materials, there are only a few examples of ACTs being conducted on metallic materials in literature [9-[*13*]. One ACT that has been conducted on metals is the small punch creep (SPC) test shown in Figure 1.*2* [14]. One advantage of this method is the small size of the specimens (approximately 10mm in diameter and .5mm thick) which proves useful when material is scarce [15]. Another advantage of the SPC is the ability to excise a sample from components in service and determine the remaining creep life of the component [14-[*16*]. A drawback of the SPC test is the physical significance of the curve regions of SPC tests are different from those from conventional creep tests [17].

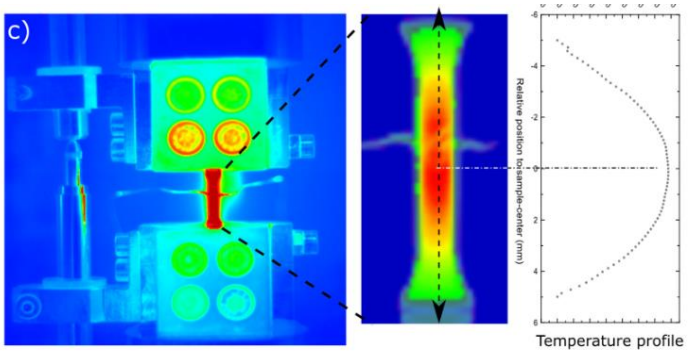

Figure 1.3 – Ultrafast creep method [18]

The ultrafast creep method is another ACT that has been used on metallic materials [18]. This method combines thermal imaging, digital image correlation (DIC), and conductive heating in order to generate multiple creep curves and various stresses and temperatures. The advantage using this method is only requiring one specimen to generate a scatter band of multiple creep rupture curves. The disadvantage of this method occurs if a thermal gradient is present within the specimen which can lead to an uncertainty of results obtained. Another disadvantage to this approach is syncing all the required sensors and machinery to gather the thermal and mechanical independently. Also, the high costs for running these experiments may deter some scientists.

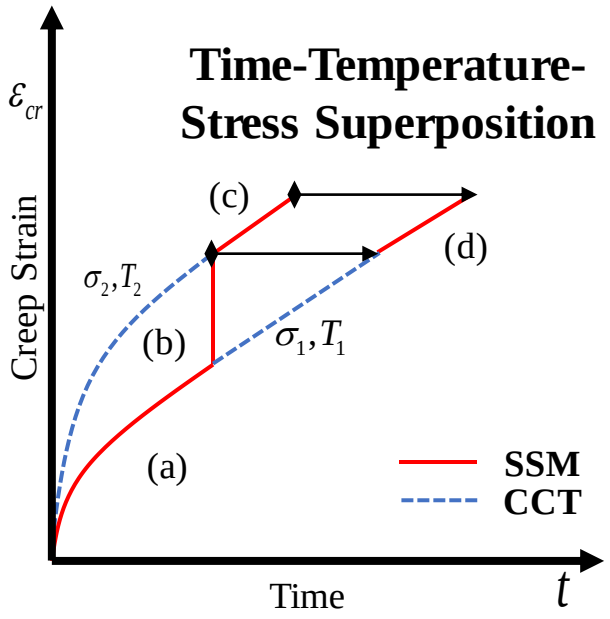

Figure 1.4 - Time-Temperature-Stress Superposition Principle (TTSSP) visualization of (a) reference stress or temperature level (b) stress or temperature step (c) elevated stress or temperature level (d) accelerated creep strain

Two proposed methods to accelerated creep testing are the time-temperature superposition principle (TTSP) and the time-stress superposition principle (TSSP). At higher temperatures and stresses, creep deformation is accelerated allowing for long-term creep properties to be gathered from short term data given adequate mathematical justification [19]. During TTSP, multiple

specimens are tested under a constant load at different temperatures resulting in separate plots of creep strain versus log (time) at different temperatures, and vice versa for TSSP where specimens are tested isothermally as shown in Figure 1.*4*. A reference temperature/stress is then selected, and all individual curves are shifted along the log (time) axis to produce a creep master curve [20-[*25*]. While TTSP and TSSP have been proven to predict creep rupture, there are several downsides to these methods. At each level of temperature/stress, there are multiple specimens used. Creep tests exhibit uncertainty where the creep response varies from specimen to specimen. The resulting accelerated creep curve then represents the aggregate uncertainty of multiple specimens. The certainty of calibration and resulting creep properties are difficult to assess [26-[*28*].

The stepped isostress method (SSM) is capable of recording over a short period of time, the long-term multistage creep deformation to rupture of materials. Where the TTSP and TSSP method require multiple specimens, the SIM and SSM tests require only one [20-[*25*, [*47*]. Each specimen is subjected to several controlled step increases of temperature/stress [29]. Having one specimen for each stress level vs having multiple specimens preserves the uncertainty of the creep response in each material. Using similar concepts from TTSP/TSSP, the stepped temperature/stress levels are segregated into individual curves and time and strain shifted to produce a creep master curve at the reference stress/temperature [30].

In response to the limited predictive capability of older models such as the Norton-Bailey law, R. W. Evan developed the Theta-projection model in 1985 [6]. The theta-projection constitutive model relies on 4 material constants and is designed to mathematically fit all 3 regimes of the classical creep curve which are shown in Chapter 4. Evans concluded that the theta projection model excels at fitting creep deformation curves for several alloys including; 1CrMoV

rotor steel, Ti.6.2.4.6, and the nickel-based superalloy IN-100, all above 700K, for a multitude of stresses [*31*].

The sin-hyperbolic (Sinh) model is a modern continuum damage mechanics (CDM)-based model for creep deformation and damage prediction [*35*-[38]. The Sinh model is introduced in Chapter 5. The model has been implemented in commercial FEA software to simulate multiaxial creep including notches and cracks. The Sinh model has also been applied to model the creep behavior of 304 stainless steel, Waspaloy, and Hastealloy X [*35*-[38].

1.3 Research Objectives

To completely validate the work for this thesis, three research objectives must be met.

Research Objective 1: Accelerated Creep Testing on Inconel 718

The objective of this study is to conduct conventional creep testing and accelerated creep testing on Inconel 718 to compare the mechanical properties of the material. It is also important to compare the microstructural images to determine if there are depletion of carbides and the formation of new phases within the material.

Research Objective 2: Application of the Theta Projection model to Accelerated Creep Data

The objective of this study is to assess the extrapolation ability of the theta projection model on accelerated creep data. The results gathered from the research objective are applied to a modified theta projection model. The data from the model is then compared to conventional creep data.

Research Objective 3: Application of the Sinh model to Accelerated Creep Data

The objective of this study is to assess the extrapolation ability of the Sinh model on accelerated creep data. Again, the results from research objective 1 are taken and applied to the Sinh model. The results from the extrapolation are then compared to conventional creep data.

1.4 Organization

The work for the present research is organized as follows. Chapter 2 introduces the material and equipment used is this study. This includes ASTM standards and the equipment used for the experiments. Chapter 3 depicts the mechanical properties and microstructure comparison of SSM and conventional creep tests as well as remarks about accelerated creep testing. Chapter 4 introduces the theta projection model applied to SSM test data and the limitations. Chapter 5 applies the same SSM test data to the Sinh model. Both model predictions are compared to conventional creep tests. Chapter 6 contains some final remarks about accelerated creep testing and ideas for future work.

CHAPTER 2: MATERIALS AND EQUIPMENT

2.1 Material: Inconel 718

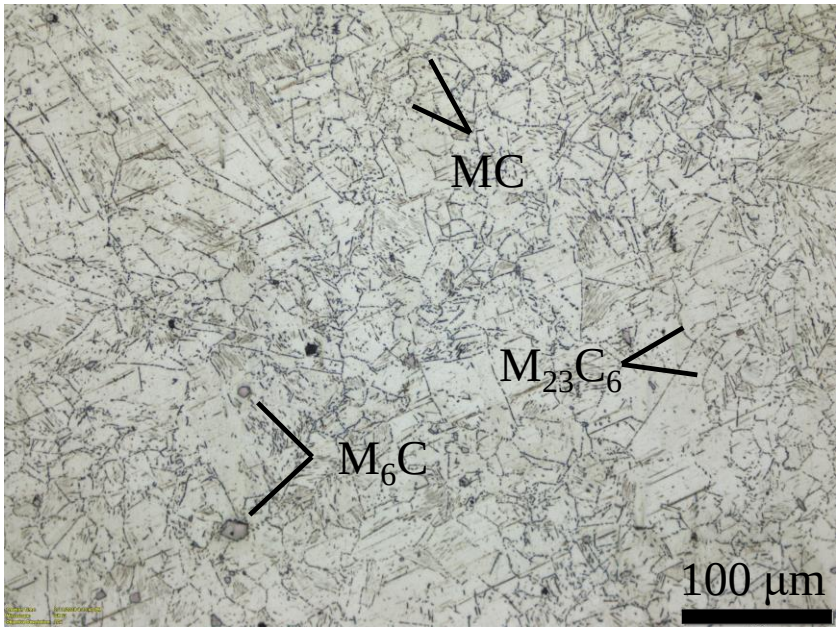

Figure 2.1 - Optical microscopy of Inconel 718 specimens

The material used for this study is non heat-treated Inconel 718 (IN 718). IN718 is a nickel-based superalloy with an austenitic (γ) face-centered cubic (FCC) crystalline structure. This material also contains FCC intermetallic compound γ' (Ni_3Al or Ni_3Ti) as well as body-centered tetragonal (BCT) γ'' precipitates (Ni_3Nb) within the γ matrix that help to strengthen the material. Several different carbides, MC, $M_{23}C_6$, M_6C, are located within the grains and grain boundaries of IN 718 which serve to increase creep resistance

[8] Mandziej, S. T. (2010). Simulative accelerated creep test on Gleeble. In Materials Science Forum (Vol. 638, pp. 2646-2651). Trans Tech Publications Ltd.

[9] Achereiner, F., Engelsing, K., Bastian, M., & Heidemeyer, P. (2013). Accelerated creep testing of polymers using the stepped isothermal method. Polymer Testing, 32(3), 447-454.

[10] Alwis, K. G. N. C., & Burgoyne, C. J. (2008). Accelerated creep testing for aramid fibres using the stepped isothermal method. Journal of materials science, 43(14), 4789-4800.

[11] Nobakhti, H., & Soltani, N. (2016). Evaluating small punch test as accelerated creep test using Larson–Miller parameter. Experimental Techniques, 40(2), 645-650.

[12] Bueno, B. D. S., Costanzi, M. A., & Zornberg, J. G. (2005). Conventional and accelerated creep tests on nonwoven needle-punched geotextiles. Geosynthetics International, 12(6), 276-287.

[13] Jeon, H. Y., Kim, S. H., & Yoo, H. K. (2002). Assessment of long-term performances of polyester geogrids by accelerated creep test. Polymer testing, 21(5), 489-495.

[14] Izaki, T., Kobayashi, T., Kusumoto, J., & Kanaya, A. (2009). A creep life assessment method for boiler pipes using small punch creep test. International Journal of Pressure Vessels and Piping, 86(9), 637-642.

[15] Nobakhti, H., & Soltani, N. (2016). Evaluating small punch test as accelerated creep test using Larson–Miller parameter. Experimental Techniques, 40(2), 645-650.

[16] Saucedo-Munoz, M. L., Komazaki, S. I., Takahashi, T., Hashida, T., & Shoji, T. (2002). Creep property measurement of service-exposed SUS 316 austenitic stainless steel by the small-punch creep-testing technique. Journal of materials research, 17(8), 1945-1953.

[17] Rouse, J. P., Cortellino, F., Sun, W., Hyde, T. H., & Shingledecker, J. (2013). Small punch creep testing: review on modelling and data interpretation. Materials Science and Technology, 29(11), 1328-1345.

[18] Barba, D., Reed, R. C., & Alabort, E. (2019). Ultrafast miniaturised assessment of high-temperature creep properties of metals. Materials Letters, 240, 287-290.

[19] Luo, W. B., Wang, C. H., & Zhao, R. G. (2007). Application of time-temperature-stress superposition principle to nonlinear creep of poly (methyl methacrylate). In Key engineering materials (Vol. 340, pp. 1091-1096). Trans Tech Publications.

[20] Schoeberle, B., Wendlandt, M., & Hierold, C. (2008). Long-term creep behavior of SU-8 membranes: Application of the time–stress superposition principle to determine the master creep compliance curve. Sensors and Actuators A: Physical, 142(1), 242-249.

[21] Giannopoulos, I. P., & Burgoyne, C. J. (2009, July). Stepped isostress method for aramid fibres. In 9th International Conference on Fiber Reinforced Polymers for Reinforced Concrete Structures (FRPRCS-9), Sydney, Australia.

[22] Giannopoulos, I. P., & Burgoyne, C. J. (2009). Stress limits for aramid fibres. Proceedings of the Institution of Civil Engineers-Structures and Buildings, 162(4), 221-232.

[23] Giannopoulos, I. P., & Burgoyne, C. J. (2011). Prediction of the long-term behaviour of high modulus fibres using the stepped isostress method (SSM). Journal of materials science, 46(24), 7660.

[24] Giannopoulos, I. P., & Burgoyne, C. J. (2012). Accelerated and real-time creep and creep-rupture results for aramid fibers. Journal of applied polyme science, 125(5), 3856-3870.

[25] Giannopoulos, I. P., & Burgoyne, C. J. (2009). Viscoelasticity of Kevlar 49 fibres. In 16th National Conference on Concrete Structures, Pafos, Cyprus.

[26] Tajvidi, M., Falk, R. H., & Hermanson, J. C. (2005). Time–temperature superposition principle applied to a kenaf-fiber/high-density polyethylene composite. Journal of applied polymer science, 97(5), 1995-2004.

[27] Vaidyanathan, T. K., Vaidyanathan, J., & Cherian, Z. (2003). Extended creep behavior of dental composites using time–temperature superposition principle. Dental Materials, 19(1), 46-53.

[28] Zornberg, J. G., Byler, B. R., & Knudsen, J. W. (2004). Creep of geotextiles using time–temperature superposition methods. Journal of geotechnical and geoenvironmental engineering, 130(11), 1158-1168.

[29] Hadid, M., Guerira, B., Bahri, M., & Zouani, A. (2014). Assessment of the stepped isostress method in the prediction of long term creep of thermoplastics. Polymer Testing, 34, 113-119.

[30] Zornberg, J. G., Byler, B. R., & Knudsen, J. W. (2004). Creep of geotextiles using time–temperature superposition methods. Journal of geotechnical and geoenvironmental engineering, 130(11), 1158-1168.

[31] Evans, R. W., & Wilshire, B. (1985). Creep of metals and alloys.

[32] Brown, S. G. R., Evans, R. W., & Wilshire, B. (1986). A comparison of extrapolation techniques for long-term creep strain and creep life prediction based on equations designed to represent creep curve shape. International Journal of Pressure Vessels and Piping, 24(3), 251-268.

[33] Brown, S. G. R., Evans, R. W., & Wilshire, B. (1986). Creep strain and creep life prediction for the cast nickel-based superalloy IN-100. Materials Science and Engineering, 84, 147-156.

[34] Evans, R. W., Parker, J. D., & Wilshire, B. (1992). The θ projection concept—A model-based approach to design and life extension of engineering plant. International Journal of Pressure vessels and piping, 50(1-3), 147-160.

[35] Stewart, C. M., 2013, "A Hybrid Constitutive Model for Creep, Fatigue, and Creep-Fatigue Damage," University of Central Florida.

[36] Haque, M. S., 2015, "An Improved Sin-Hyperbolic Constitutive Model for Creep Deformation and Damage," The University of Texas at El Paso.

[37] Haque, M. S., and Stewart, C. M., 2016, "Finite-Element Analysis of Waspaloy Using Sinh Creep-Damage Constitutive Model Under Triaxial Stress State," J. Press. Vessel Technol. Trans. ASME, 138(3), pp. 1–9.

[38] Haque, M. S., and Stewart, C. M., 2016, "Exploiting Functional Relationships Between MPC Omega, Theta, and Sine-Hyperbolic Continuum Damage Mechanics Model," *Proceedings of ASME 2016 Pressure Vessels and Piping Conference PVP 2016*, Vancouver, British Columbia, Canada, pp. 1–11.

[*39*]. Specimens were etched with Kalling's No.2 and initial optical images are shown in Figure 2.1 [40].

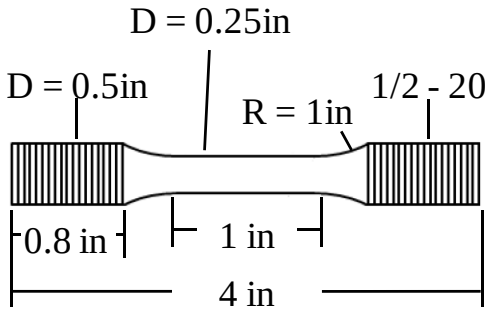

Figure 2.2 – Specimen dimensions for testing

The heat was initially melted using a vacuum induction melting (VIM) and electroslag remelting (ESR) processes. The heat was subjected to a solution annealing heat-treatment at 955°C for 1 hour and then water quenched. The nominal, mill test report (MTR), and X-ray fluorescence (XRF) chemical compositions are reported in Table 2.*1*. Specimens were machined a gauge length of 1 inch and a gauge diameter of .25 inches, and were prepared in accordance with ASTM E8 and ASTM 139 and shown in Figure 2.*2* [41[*42*].

Table 2.1: Chemical composition (wt%) of Inconel 718 [43]

Element	Nominal	MTR	XRF
Ni	50-55	52.55	51.24
Cr	17-21	18.52	18.40
Fe	Bal*	18.2	19.25
Nb	4.75-5.50	5.2	4.94
Mo	2.80-3.30	2.92	2.85
Ti	0.65-1.15	0.93	1.28
Al	0.20-0.80	0.52	0.50
Co	1	0.52	0.54
C	0.08	0.04	--
Mn	0.35	0.05	0.17
Si	0.35	0.08	--
P	0.015	0.007	--
S	0.015	0.0005	--
B	0.006	0.004	--

Cu	0.3	0.05	--

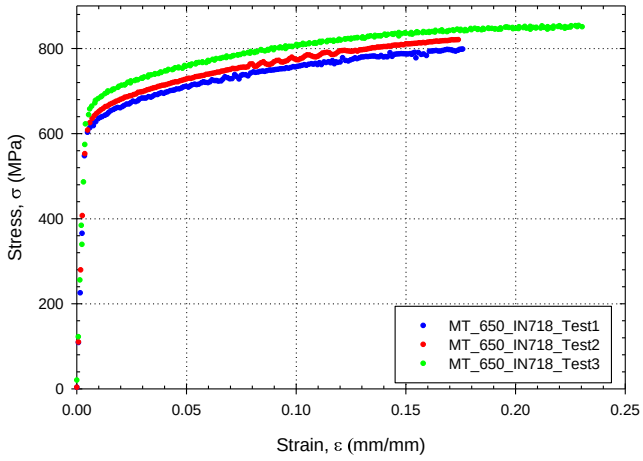

Figure 2.3 – Stress-strain curves of IN 718

Three monotonic tensile tests were performed on the IN 718 material at 650°C, conforming to ASTM E21 [44]. The resulting stress-strain curves are shown in Figure 2.3. The ultimate tensile strengths, .2% offset yield strengths, Young's moduli, and elongations are labeled in Table 2.2.

Table 2.2: Monotonic tensile properties of IN 718 at 650°C

	Tensile Strength, σ_{UTS} (MPa)	Yield Strength, σ_{YS} (MPa)	Modulus, E (GPa)	Elongation (%)
Test 1	798.6	613.6	157.1	17.6
Test 2	820.6	625.3	153.4	17.4
Test 3	854.1	664.3	147.5	23.0
Average	824.4	634.4	152.7	19.3
COV	3.38	4.18	3.17	16.4

2.2 Equipment

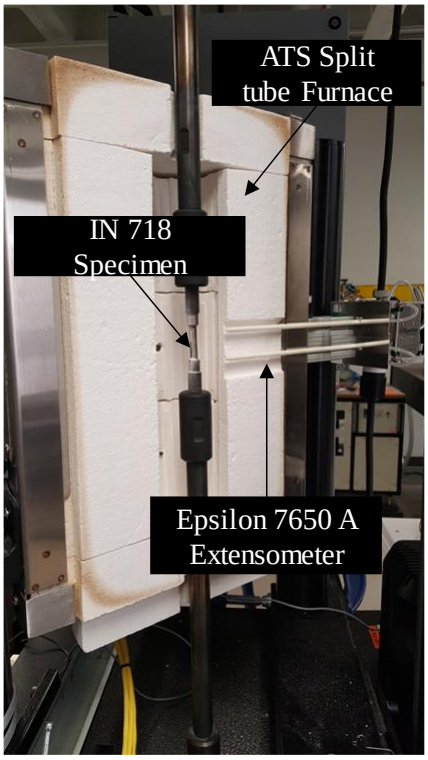

Figure 2.4 – Experimental setup for mechanical testing in Instron 5969

All mechanical tests in this study were performed using an Instron 5969 Universal Testing System with a 50kN load cell. Strain measurements were captured using an Epsilon 7650A high temperature low strain extensometer. The extensometer meets ASTM E83 class A with a 1 in gauge section and measures up to 10% strain. Temperature was controlled using an Applied Testing Systems three zone split tube furnace with a Watlow PM digital controller. A K-type thermocouple is welded to the center of the gauge section of each specimen using a HotSpot II thermocouple welder and monitored using a CSi32 Omega Miniature Benchtop Controller. Experimental setups are shown in Figure 2.*4*.

CHAPTER 3: ACCELERATED CREEP TESTING

3.1 Experiments

Conventional creep tests are performed according to ASTM E139 [42]. A test matrix for the CCTs is listed in Table 3.1. The CCT tests are performed to post-audit validate the SSM approach when applying the McVetty and Sinh constitutive models. The creep tests were designed to within 168 hours.

Table 3.1: Test matrix for CCT tests

Temp. (°C)	Stress (MPa)	Repeats
650	636	3

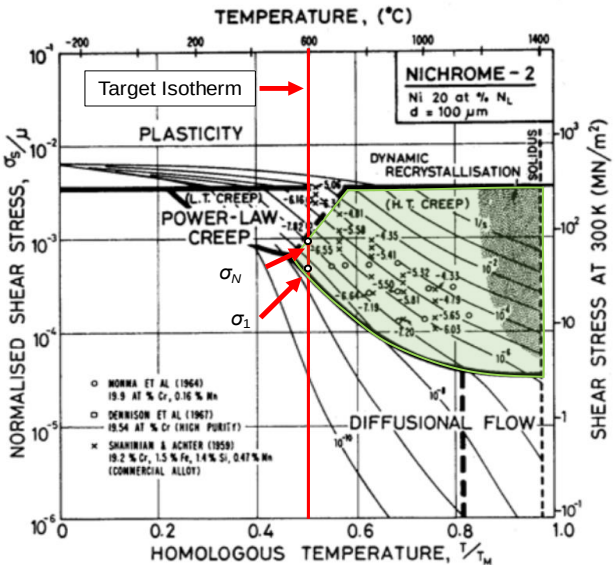

Figure 3.1 – Deformation Mechanism Map of Nickel 20%Chromium Alloy [45]

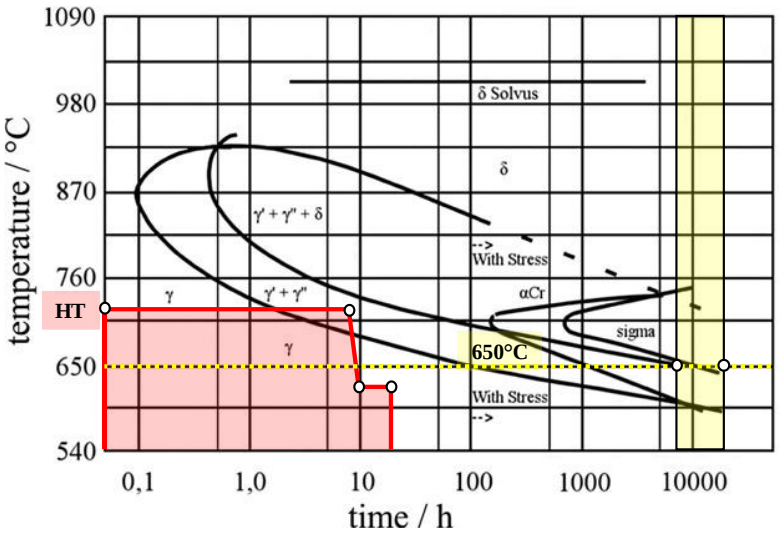

Figure 3.2 – Time-Temperature-Transformation Diagram of IN718

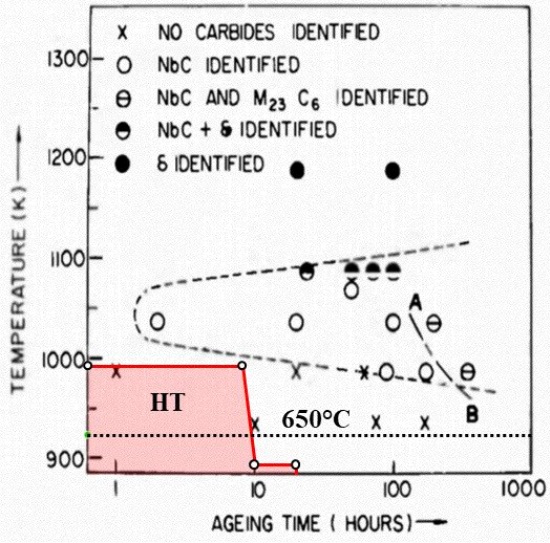

Figure 3.3 – Time-Temperature-Phase Diagram of IN718

When designing an ACT, it is important to look at the material that will be used and gather the necessary information from deformation mechanism maps, time-temperature-transformation diagrams (TTT), and time-temperature-phase (TTP) diagrams of the material in question. It is important to look at deformation mechanism maps because this will tell how a material is going to deform at various temperatures and stresses. The reason this is important is because a user needs to ensure only one mechanism is chosen. In the case for these experiments, there was no deformation map for IN718, however, there was one with similar properties shown in Figure 3.*1*.

These experiments ran in the high temperature creep regime. It is also important to look at TTT and TTP diagrams when designing an ACT, because failure of a material begins at the microstructure. At these extreme environments, carbides and phases can either form or deplete depending on the material. In the case for IN718, Figure 3.*2* and Figure 3.*3* depict the change in the γ matrix and which carbides form. At 650°C, δ will not form until after 1000 hours, and no new carbides are expected. For this study, the stepped isostress method was the ACT that was chosen for these sets of experiments. While both experiments, SSM and SIM, have rarely been applied to metallic materials, it is easier to control an experiment by load rather than by temperature.

The SSM tests are performed at a reference stress level and are stepped by increasing stress levels with a fixed magnitude at a fixed hold duration. Because the conventional creep tests were conducted at 636MPa, the initial stress the SSM experiments will begin at 636 MPa as well. The hold duration should be minimized but encompass the minimum creep strain rate at the reference stress level. The final stress level should be maintained until rupture. The duration of the transitions between stress levels should be as short as possible while avoiding shock forces. A test matrix of the SSM experiments is listed in Table 3.2. The results from the CCTs and SSM are shown in the following chapters as they are applied to the McVetty and Sinh constitutive models.

Table 3.2: Test matrix for SSM tests

Temp., T (°C)	Stress Levels, σ_i (MPa)	Magnitude of Stress Step, $\Delta\sigma$ (MPa)	Hold duration, Δt (hr)	Repeats
650	636, 681, 726, 771	45	5	3

3.2 CCT and SSM Results

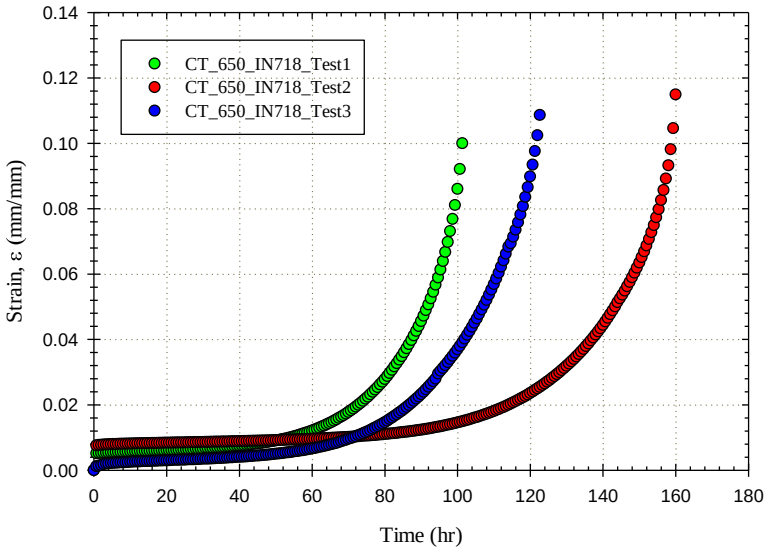

Figure 3.4 – Results from CCT experiments on IN718 at 650°C

Three CCT experiments were conducted on the specimens in order to capture any uncertainty due to creep as shown in Figure 3.4. The short-term creep data was also used to act as the high-resolution data needed to be quantitively compared to the ACTs to determine the overall quality of the calibration approaches. Table 3.3 depicts the data from the CCT experiments.

Table 3.3: Data for conventional creep testing of IN718

Specimen ID	Testing Temperature (°C)	Rupture Time (hr)	Final Stress (MPa)	Final Creep Strain (%)	Minimum-Creep-Strain Rate	Adjusted Elastic and Plastic Creep Strain
CCT_650_IN718_Test1	650	101.3	771	10.0	3.04E-04	.0042
CCT_650_IN718_Test2	650	160.3	725	12.7	4.19E-04	.0061
CCT_650_IN718_Test3	650	123.2	725	11.6	4.90E-05	.0052
Coefficient of Variance	-	23.25	3.58	11.87	73.59	18.40

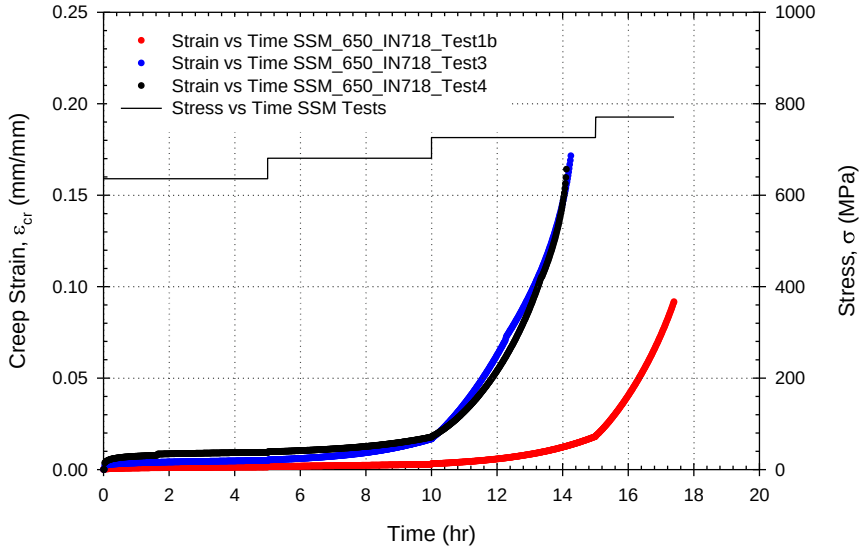

Figure 3.5 – Results from SSM experiments on IN718 at 650°C

Three SSM experiments were conducted in order to capture any uncertainty with the ACT. It should be noted that tests 3 and 4 failed at the third step of the experiments while test 1b failed at the fourth step as shown in Figure 3.5. It should be noted the number of steps a user selects do not matter as this is not a rule mentioned in literature. The coefficient of variance for the rupture between the 3 SSM experiments is smaller when compared to the 3 CT experiments, however, the coefficient of variance for the final creep strain for the SSM experiments is smaller than the CT experiments.

Table 3.4: Stepped Isostress Data of IN718

Specimen ID	Testing Temperature (°C)	Rupture Time (hr)	Final Stress (MPa)	Final Creep Strain (%)
SSM_650_IN718_Test1b	650	17.4	771	10.0
SSM_650_IN718_Test3	650	14.3	725	17.2
SSM_650_IN718_Test4	650	14.1	725	16.4
Coefficient of Variance	-	12.11	3.58	27.15

3.3 Microstructural Comparison

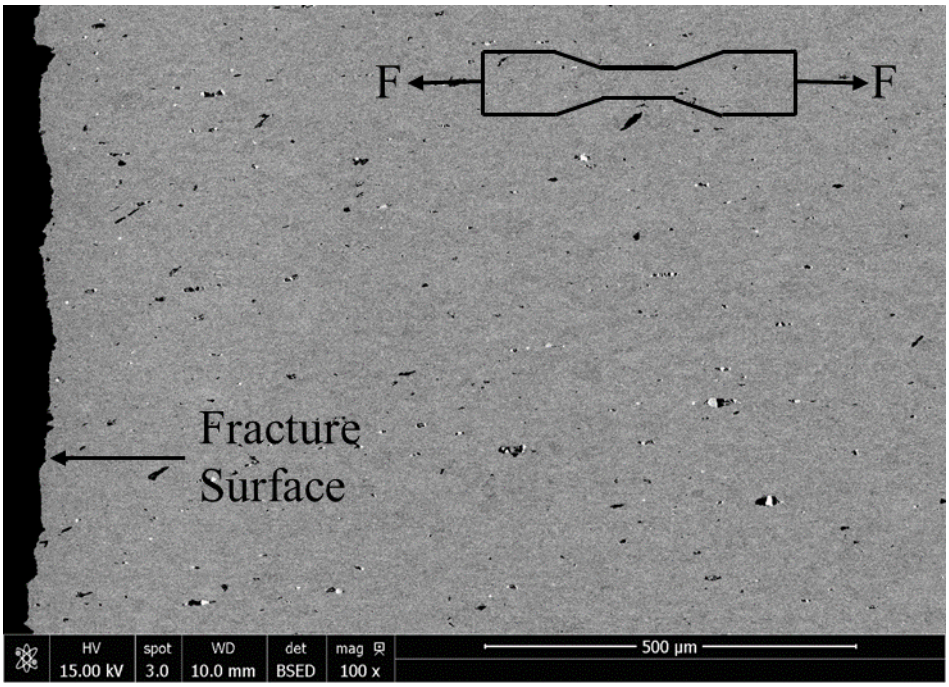

Figure 3.6 – SEM backscatter image of conventional creep testing

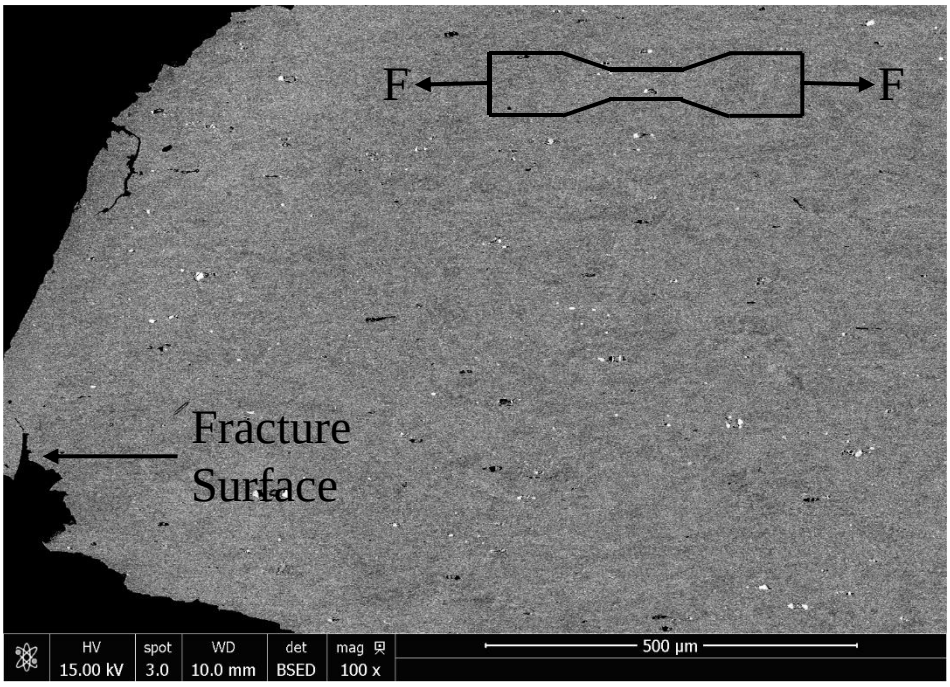

Figure 3.7 – SEM backscatter image of stepped isostress method

For accelerated creep testing to be accepted, it is important for the microstructure of the material to be consistent with that of conventional creep testing. There are some differences in the microstructures, which can lead to improvements of the ACT design on a new round of experiments as shown in Figure 3.*6* and Figure 3.*7*. For conventional creep testing, void formation is much more prevalent when compared to the SSM experiment. The reason for this difference is that the load for conventional creep testing was constant while for SSM each step was getting closer to the ultimate tensile strength of the material. This is also shown at the fracture surface of both images. In chapter 6, it will be discussed how improvements can be made to these experiments.

CHAPTER 4: APPLICATION OF THE THETA PROJECTION MODEL TO ACT DATA

4.1 Theta Projection Model

The Theta-projection model is as follows

$$\varepsilon = \theta_1(1-\exp(-\theta_2 t)) + \theta_3(\exp(\theta_4 t)-1) \quad (1)$$

where θ_1, θ_2, θ_3, and θ_4 are four material constant measured in %-strain/hr that are designed to mathematically fit all three creep stages [31[*34*]. The equation is composed of two parts as follows

$$\varepsilon_{pr} = \theta_1(1-\exp(-\theta_2 t)) \quad (2)$$

$$\varepsilon_{tr} = \theta_3(\exp(\theta_4 t)-1) \quad (3)$$

where [Eq.(2)] is a time hardening equation for the primary stage of creep and [Eq.(3)] is a time softening equation for the tertiary stage of creep. θ_1 determines the magnitude while θ_2 determines the exponential decay as creep transitions into the secondary regime. θ_3 determines the magnitude while θ_4 determines the exponential acceleration of strain to fracture.

4.2 Methodology

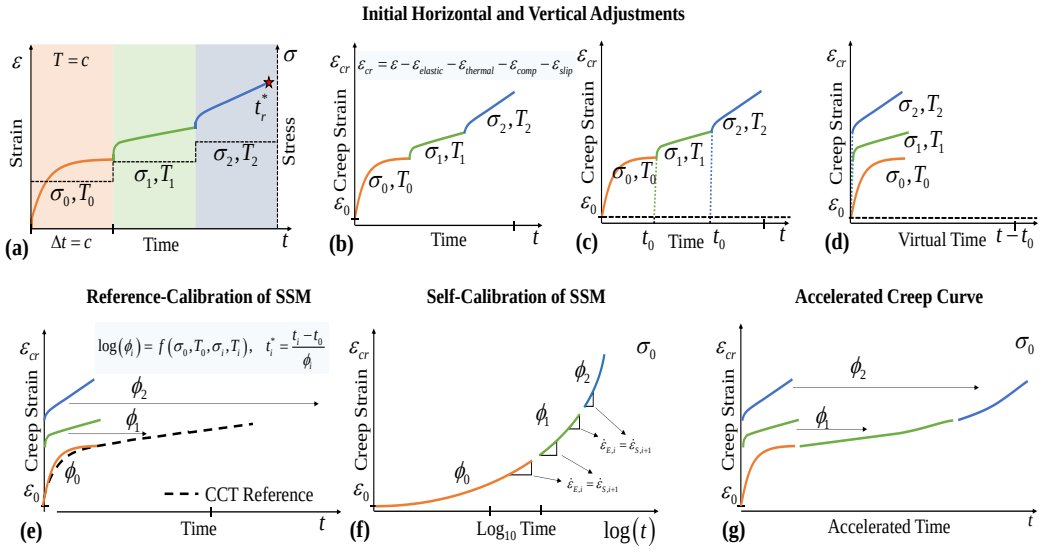

Figure 4.1 – Depiction of how constitutive models are applied to accelerated creep data: (a) gathering of SSM results, (b) removal of elastic, plastic, thermal strains to ensure only creep strain, (c) location of the virtual start time at each step, (d) zeroing at each start time, (e) user applies a polynomial like what is done in literature to fit data and generate a master curve, (f) application of constitutive model and calibrating material constants (g) generation of creep master curve

Application of any constitutive model to accelerated creep data must go through a methodological approach as shown in Figure 4.*1*. The first step to this is gathering the ACT data. The next step is to subtract all of the strains that accumulated during the experiment to find the creep strain of the specimen. The following step is to find all of the virtual start times of each step and zero them out. From here the user has two choices to generate a creep master curve. The first approach is using reference calibration, which is commonly used in literature, to apply a polynomial and generate a master curve. This approach is more of a curve fitting approach as the need for existing creep data is needed to generate these curves, which is unwanted as ACTs need to be independent from any existing creep data. The second approach is the self-calibration approach which is preferred because a constitutive model is used to find material constants based on the equation that is used. This approach does not require any preexisting creep data.

The self-calibration method for applying the theta projection model to SSM is divided into three steps: the creep strain adjustment, the virtual start time adjustment, and the time-shift adjustment.

Step 1 – Creep Strain Adjustment

When conducting SSM tests, the total strain from the experiment is given. Before the virtual start time and time-shift adjustments can be determined, the creep strain must be calculated. The creep strain, ε_{cr} is calculated from the measured total strain, ε by rearrangement as follows

$$\varepsilon_{cr} = \varepsilon - \varepsilon_{elastic} - \varepsilon_{plastic} \tag{4}$$

where $\varepsilon_{elastic}$ is elastic strain, $\varepsilon_{plastic}$ is rate-independent plastic strain, and ε_{misc} are miscellaneous strains due to equipment compliance, unrelieved thermal strains, and others. The resulting adjusted creep strain curve is depicted in Figure 4.*1*(b). Elastic strain is calculated using Hooke's law, while plastic strain is calculated using the .2% offset line gathered from separate monotonic tests of the material.

Step 2 – Virtual Start Time Adjustment

The virtual start time adjustment converts the measured continuous creep deformation curve into a series of individual creep deformation curves. This is achieved by calculating a virtual start time, t_0, as if the curve for each stress level was produced from an independent, initially unloaded creep test. The virtual start time, t_0 is obtained by fitting a constitutive law to each stress/temperature level and then shifting the individual temperature/stress levels to zero time as shown in Figure 4.*1*(d). The existing approach is to fit a polynomial equivalent to Graham-Walles or a Prony series to the data [19]. In the self-calibration approach, constitutive models are recommended. The following rules for the constitutive models must be enforced:

- Be able to model primary, secondary, and tertiary creep. Ideally, the regimes should be separated into independent functions such that the model can be simplified to better fit the given stress level. For instance, if there is no tertiary creep regime at a stress level, the function associated with tertiary creep should be zeroed out to increase the statistical dependencies of the material constants for primary and secondary regimes.
- Be able to predict zero strain at a non-zero time. In most models, this can be enabled by replacing t with $(t-t_0)$ everywhere; however, care must be taken to prevent the constitutive model from becoming over-defined. Zeroing out unnecessary creep regimes can help mitigate this issue.

In this study, a modified Theta Projection constitutive model is applied in the following form

$$\varepsilon = \theta_1(1-\exp(-\theta_2(t-t_0))) + \theta_3(\exp(\theta_4(t-t_0))-1) \tag{5}$$

where ε is the creep strain, t is the time, t_0 is the virtual start time, and $\theta_1, \theta_2, \theta_3,$ and θ_4 are scaling and rating parameters for the primary and tertiary creep regimes [46].The model is also able to predict zero strain from a non-zero time while remaining well-defined. Taking the derivative of creep strain [Eq. (5)] with respect to time provides the creep strain rate:

$$\dot{\varepsilon}_{cr} = \theta_1\theta_2 \exp(-\theta_2(t-t_0)) + \theta_3\theta_4 \exp(\theta_4(t-t_0)) \tag{6}$$

where due to the exponential functions, the form remains simple.

Step 3 – Time-Shift Adjustment

The time-shift adjustment converts the individual creep deformation curves into a single accelerated creep deformation curve. This is achieved by calculating time-shift factors, ϕ_i, for each stress level.

In conventional creep tests, the creep strain rate does not exhibit a dramatic change in rate; rather, the rate evolves as a continuous decreasing or increasing function with respect to primary and tertiary creep regimes, respectively. If the steps between stress levels remain moderate, the time-shift factors can be obtained from creep strain rate match. In this case, the time between stress levels is 5 hours until rupture. Accelerating SSM data using creep strain rate matching between the stress level is as follows

$$\dot{\varepsilon}_{E,i}{}^{*} = \dot{\varepsilon}_{S,i+1}{}^{*} \tag{7}$$

where $\dot{\varepsilon}_{E,i}{}^{*}$ is the accelerated creep strain rate of the end of the i^{th} stress level, and $\dot{\varepsilon}_{S+i}$ is the accelerated creep strain rate of the beginning of the $i^{th}+1$ stress level. This relationship can be restated in incremental form as follows

$$\frac{\Delta\varepsilon_{E,i}}{\Delta t^{*}_{E,i}} = \frac{\Delta\varepsilon_{S,i+1}}{\Delta t^{*}_{S,i+1}} \tag{8}$$

where acceleration arises due to an acceleration of the time increment Δt^{*}. The accelerated time is expressed as follows

$$t^{*}_{i} = \frac{t_i - t_{0,i}}{\phi_i} \tag{9}$$

where t_i is the time for each stress step, t_0 is the virtual start time adjustment calculated in step 2, and ϕ_i is the time shift adjustment for the i^{th} stress level. When introduced into the incremental form as seen in [Eq.(8)], the strain rates become

$$\frac{\Delta\varepsilon_{E,i}\cdot\phi_i}{\Delta t_i} = \frac{\Delta\varepsilon_{S,i+1}\cdot\phi_{i+1}}{\Delta t_{i+1}} \tag{10}$$

where ϕ_{i+1} is the time-shift factor corresponding to the $i+1$ stress level. This can be simplified into

$$\phi_i \cdot \dot{\varepsilon}_{E,i} = \phi_{i+1} \cdot \dot{\varepsilon}_{S,i+1} \tag{11}$$

The timeshift factors can then be determined directly as follows

$$\phi_{i+1} = \frac{\phi_i \cdot \dot{\varepsilon}_{E,i}}{\dot{\varepsilon}_{S,i+1}} \tag{12}$$

where the first time-shift factor in all exponents is $\phi_1 = 1$.

Unfortunately, experimental creep strain rate data fluctuates too much to produce reliable ϕ values. Instead, the calibrated modified-theta model rate as seen in [Eq.(5)] is employed. In practice, it is best to numerically solve [Eq.(9)] with [Eq.(5)] embedded over an overlapping range of real time. This produces a more realistic and continuous accelerated creep curve.

The calibration of time-shift factors is extremely sensitive to the selected overlapping time interval in materials that exhibit a prominent primary creep regime. This sensitivity is illustrated in Figure 4.*1*(f) using a linear function in lieu of [Eq.(5)] for simplicity of interpretation.

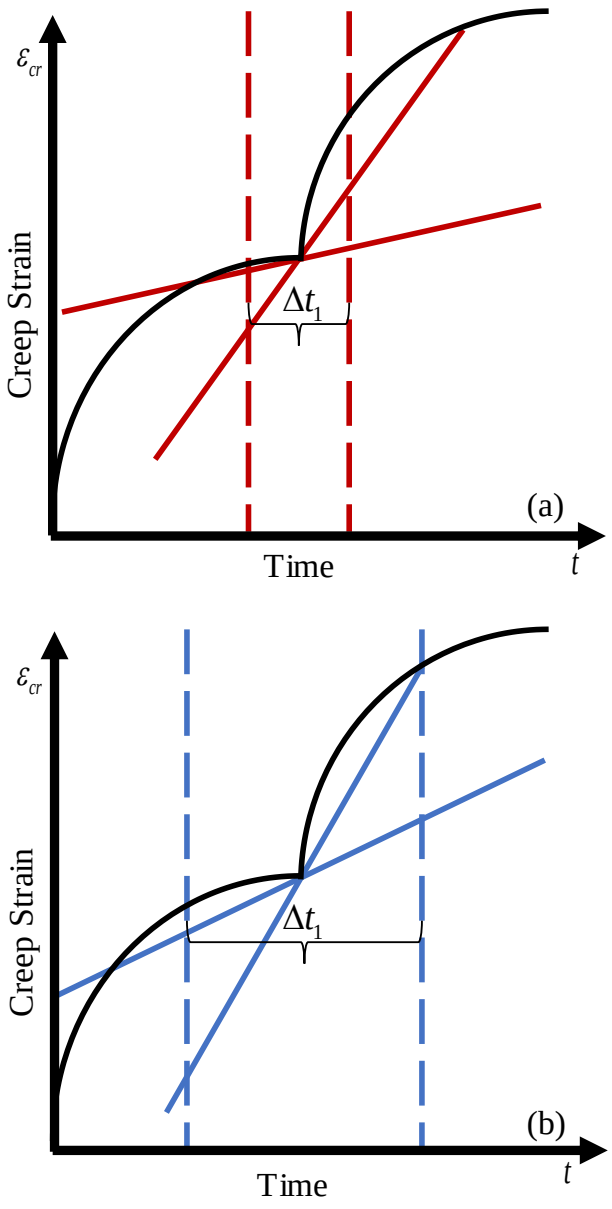

Figure 4.2 - Illustration of time-shift sensitivity issues for (a) a narrow and (b) wide time overlap

When a narrow time interval is employed as shown in Figure 4.*2*(a), the difference slope between stress levels is maximized resulting in greater acceleration while with a wider time interval as shown in Figure 4.*2*(b), the slopes not as far apart resulting in less acceleration. This problem would disappear in materials that exhibit little to no primary creep. This problem can exacerbate by accounting for time-independent plasticity when operating above the yield strength

of a material. As a consequence of this issue, the time interval must be calibrated specific-to-material.

4.3 MATLAB Code

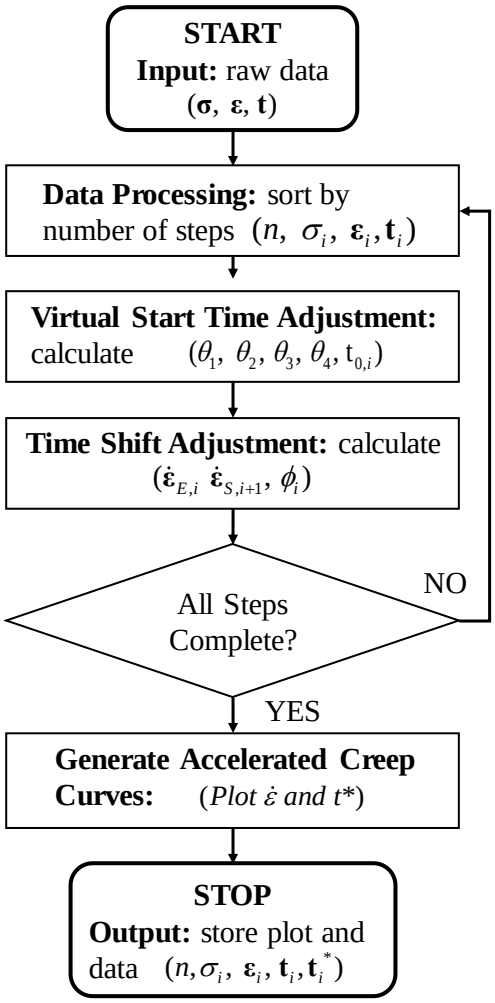

Figure 4.3 - MATLAB Code Map for Theta Projection

To generate the accelerated creep curves, a MATLAB code was written as outlined in Figure 4.3. The code is divided into five subroutines and is currently configured to accelerate one SSM test at a time. The algorithm starts with reading the SSM data (stress, creep strain, and time) into MATLAB. The data is processed to identify the number of stress steps, creep strain at each level of stress, and the real time for each level. For each stress step, the modified Theta constitutive

law [Eq.(5)] is calibrated (using nonlinear least squares) to obtain the material constants, but more importantly the virtual start time, unique to each stress level. Next, for each stress step, the time shift factor, is obtained (using nonlinear least squares) according to the self-calibration approach described in the previous section. Finally, the accelerated time, is calculated for each stress level and the accelerated creep curve generated. The last subroutine exports all data generated in the acceleration process as well as the squared residual norm, of the nonlinear--least--squares routines.

4.4 Results

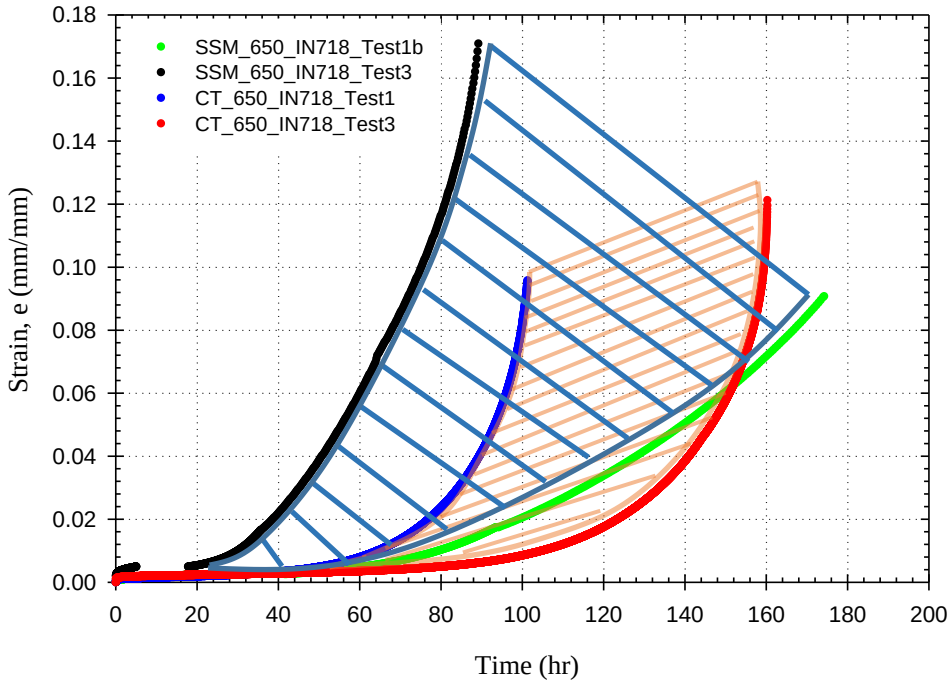

Figure 4.4 – Comparison of Theta Projection with Conventional Creep Tests

The results from the ACT data are depicted in Figure 4.*4* and the material constants are show in Table 4.1. It can be observed that the theta projection model either underpredicts or overpredicts creep rupture behavior when compared to the conventional creep data. This may be caused by the models lack of ability to model accurately the secondary creep regime due to the

first part of the equation modeling primary creep and the second part of the equation modeling secondary creep as shown in [Eqs.(1)-(3)]. Another issue is accurately finding the ϕs. Because a user can determine how much time is needed for the strain rate matching, and this can be difficult to accurately generate a master curve.

Table 4.1: Accelerated SSM Data at 650°C

Specimen ID	Temperature (°C)	Rupture Time (hr)	Creep Ductility (%)	$t_{0,2}$	$t_{0,3}$	$t_{0,4}$	ϕ_1	ϕ_2	ϕ_3	ϕ_4
SSM_650_IN718_Test1b	650	174.2	9.1	3.7	6.0	12.2	1	.31	.09	.02
SSM_650_IN718_Test3	650	101.3	17.2	4.4	7.7	-	1	.58	.14	-

CHAPTER 5: APPLICATION OF THE SINH MODEL TO THE SSM TESTS

5.1 Sinh Model

The Sine hyperbolic (Sinh) model is a continuum damage mechanics (CDM) model which was developed to model the secondary and tertiary stages of creep [35-[38]. The Sinh model equations are as follows

$$\dot{\varepsilon}_{cr} = A\sinh\left(\frac{\sigma}{\sigma_s}\right)\exp(\lambda\omega) \tag{13}$$

$$\dot{\omega} = \frac{M(1-\exp(-\phi))}{\phi}\sinh\left(\frac{\sigma}{\sigma_t}\right)^{\chi}\exp(\phi\omega) \tag{14}$$

$$\omega(t) = -\frac{1}{\phi}\ln\left[1-[1-\exp(\phi)]\frac{t}{t_r}\right] \tag{15}$$

where $A, \sigma_s, \lambda, M, \sigma_t$, and χ are material constants, σ is stress, t_r is rupture, ω is damage; an internal state variable that evolves from an initial damage to unity and ϕ is a constant that controls the damage trajectory and may be stress and/or temperature dependent.

5.2 Methodology

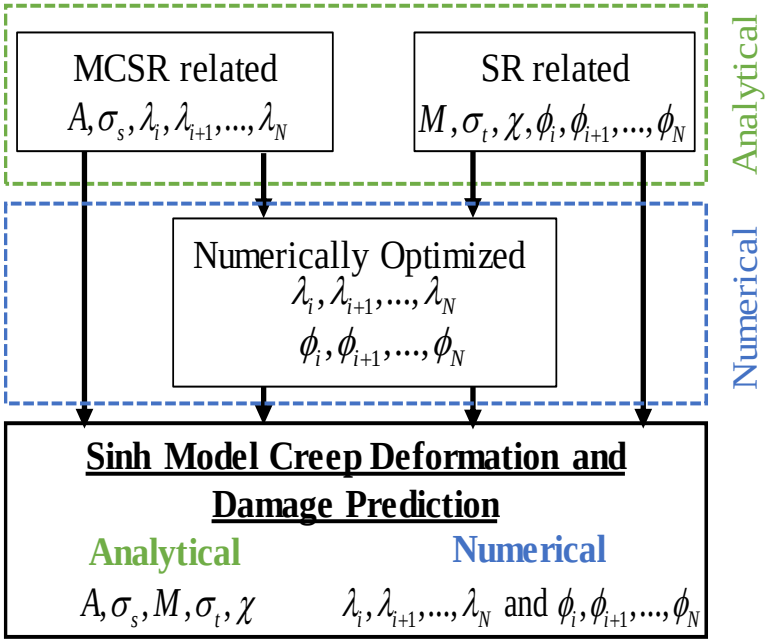

Figure 5.1 – An illustration of the calibration approach by Sinh model for SSM test data

The steps to applying the Sinh model are the same as what was mentioned in the previous chapter. The only difference is instead of applying the Theta Projection model, the Sinh model is applied. Calibration of the Sinh model material constants is performed to portray the accuracy of the Sinh in predicting the creep deformation to rupture. The calibration of the SSM test data begins with the determination of the material constants in the Sinh coupled constitutive equation. The Sinh model take 7 material constants $(A, \sigma_s, \lambda, M, \sigma_t, \chi, \phi)$ into the constitutive equations. An illustration of the calibration approach adopted in this study is shown in Figure 5.1. The calibration approach is twofold: Analytical and Numerical.

Minimum Creep Strain Rate Constant

The first step of the calibration approach is the determination of MCSR related constants. Sinh CSR equation [Eq.(13)] for SSM is can be stated as follows

$$\dot{\varepsilon}_{cr} = A\sinh\left(\frac{\sigma_i}{\sigma_s}\right)\exp(\lambda_i\omega) \tag{16}$$

where, *i* denotes the stress level of interest. Material constant A and σ_s are scalar and assumed to be independent of stress or damage variation. Material constant λ is a vector (variable as step changes) and dependent of stress and/or damage accumulation. Constitutive Damage Mechanism laws state that, at the beginning damage is zero $(\omega = 0)$ and at the rupture damage reached to unity $(\omega = 1)$. These two states are exploited to form the following equations

$$\dot{\varepsilon}_{\min} = A\sinh\left(\frac{\sigma_1}{\sigma_s}\right) \tag{17}$$

$$\dot{\varepsilon}_{final} = A\sinh\left(\frac{\sigma_N}{\sigma_s}\right)\exp(\lambda_N) \tag{18}$$

$$\lambda_N = \ln\left(\frac{\dot{\varepsilon}_{final}}{\dot{\varepsilon}_{\min}}\right) \tag{19}$$

where, N denotes material constants at the final stress level and σ_1 is the initial stress. The minimum $(\dot{\varepsilon}_{\min})$ and final $(\dot{\varepsilon}_{final})$ creep strain rate are determined directly from the experimental data. These 3 equation are solved analytically to find the material constant A, σ_s, and λ_N. Next step is to calibrate the remaining material constant, λ and damage vector, ω across the stress levels. The Sinh CSR [Eq. (13)] is rearranged to the following form.

$$\lambda_i\omega = \ln\left(\frac{\dot{\varepsilon}_{cr}}{A\sinh\left(\frac{\sigma_i}{\sigma_s}\right)}\right) \tag{20}$$

The non-separable $\lambda_i\omega$ is calculated with employing the [Eq. (20)]. The λ and ω is separated and a simulated magnitude is calibrated for both. An objective function is employed to optimize the simulated value for λ and ω setting the following constraints.

$$\begin{aligned} &\lambda_i > \lambda_{i-1} > \ldots > \lambda_N \\ &0 \le \lambda_i \le \ln(\infty) \\ &0 \le \omega \le 1 \end{aligned} \tag{21}$$

The analytically calibrated MCSR related material constants are reported in Table 5.2. Note that, the analytically evaluated material constant, λ is later numerically refined to fit the model through the data.

Stress Rupture Constants

In this section the SR related material constants are calibrated. The first step is to generate the damage evolution curve. The damage curve can be obtained using the calibration approach adopted in the previous section. The sudden introduction of this plastic damage has the effect of reducing the creep resistance of the material. For each SSM test, final damage accumulation is the sum of creep and instant plastic damage.

The next step is to employ the Sinh damage rate equation [Eq.(13)] to calibrate the SR related material constants. Sinh damage rate equation [Eq.(13)] can be stated as follows for SSM

$$\dot{\omega} = \frac{M[1-\exp(-\phi_i)]}{\phi_i} \sinh\left(\frac{\sigma_i}{\sigma_t}\right)^{\chi} \exp(\phi_i \omega) \tag{22}$$

where, *i* denotes the stress level of interest. Material constant M, σ_t, and χ are scalar and assumed to be independent of stress and/or damage accumulation. Material constant, ϕ_i is vector and dependent of the stress and/or damage accumulation. A similar framework is developed here like the previous section to calibrate SR related material constant. Exploiting the CDM laws, the following 4 equations can be formulated

$$\omega_{c,1} = -\frac{1}{\phi}\ln\left[1-[1-\exp(-\phi)]\frac{t_1}{\left[M\sinh\left(\frac{\sigma_1}{\sigma_t}\right)^{\chi}\right]^{-1}}\right] \tag{23}$$

$$\dot{\omega}_o = \frac{1-\exp(-\phi_1)}{\phi_1} M\sinh\left(\frac{\sigma_1}{\sigma_t}\right)^{\chi} \tag{24}$$

$$\dot{\omega}_f = \frac{1-\exp(-\phi_N)}{\phi_N} M\sinh\left(\frac{\sigma_N}{\sigma_t}\right)^{\chi} \exp(\phi_N) \tag{25}$$

$$\phi_N = \ln\left(\frac{\dot{\omega}_o}{\dot{\omega}_f}\right) \tag{26}$$

where, N denotes the materials constants at the final stress level, $\omega_{c,i}$ is creep damage accumulated at the first step, $\dot{\omega}_o$ and $\dot{\omega}_f$ is the initial and final damage rate respectively, and σ_1 is the stress level of first step.

To calibrate the material constant ϕ_1, [Eq.**Error! Reference source not found.**] and [Eq. **Error! Reference source not found.**] are combined and rearranged to following form

$$\omega_{c,1} = -\frac{1}{\phi}\ln\left[1-\left[1-\exp(\phi)\right]\frac{t_1\phi_1\dot{\omega}_o}{1-\exp(-\phi_1)}\right] \tag{27}$$

Solving [Eq.(27)], the material constant ϕ_1 is calibrated.

The remaining equation [Eqs. (23)-(26)] are solved to calibrate the material constant, M, σ_t, χ, and ϕ_N by setting the following constraints.

$$\begin{aligned} &\phi_i > \phi_{i-1} > ... > \phi_N \\ &0 \le \phi_i \le \ln(\infty) \\ &0 \le \sigma_t \le \sigma_{UTS} \\ &\text{M>0} \end{aligned} \tag{28}$$

The analytically calibrated material constants are reported in Table 5.2. To find the intermediate ϕ constants $(\phi_{i+1}, \phi_{i+2}, ..., \phi_{N-1})$, a numerical approach is adopted. An objective function is employed and optimized to find the best-fitted ϕ for each load steps.

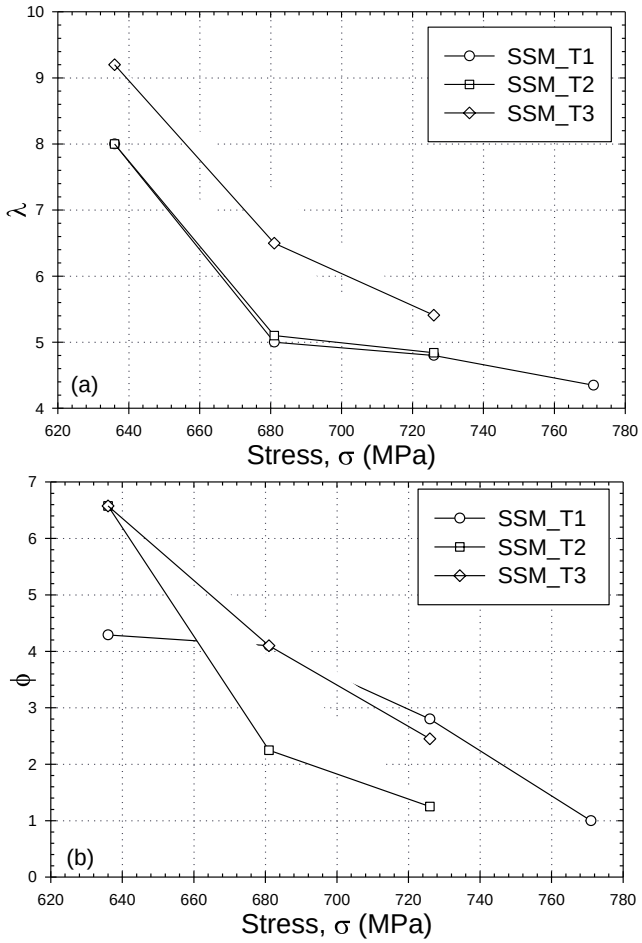

Figure 5.2 - Calibrated (a) λ and (b) ϕ for triplicate SSM across multiple stress at 650°C

The numerically refined material constants, λ and ϕ for triplicate SSM test are plotted to illustrate the strong stress dependency in Figure 5.2. Both λ and ϕ show a decreasing trend with

the increasing stress. For material constant, λ, higher stress leads to higher ductility and shorter rupture life and vice versa for material constant ϕ.

5.3 Results

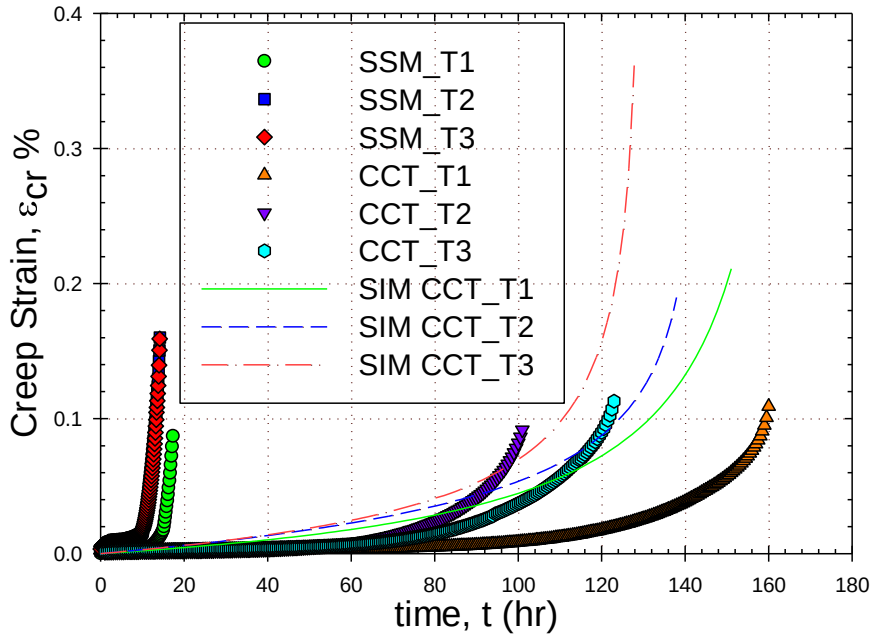

Figure 5.3 - Comparison of Sinh extrapolated CCTs with experimental CCTs and SSMs

The material constants for each the experiments are depicted in Table 5.1. The Sinh fit accords well with the experimental SSM data as seen in Figure 5.3. The model also exhibits the ability to predict the damage evolution from zero to unity across multiple stresses. The damage evolution curves show instantaneous plasticity attributed to repeated yielding of the test specimen. This introduction of plastic damage along with the creep damage leads to quick rupture of the specimen, leading to shorter test duration. This is also the reason why the ductility of the Sinh predictions are higher than the conventional creep tests. The Sinh model damage prediction accounts for the induced plastic damage as shown in the Table 5.3.

Table 5.2: Analytically calibrated material constants of Sinh for triplicate SSM at 650°C

Test ID	A $\%hr^{-1}\times10^{-7}$	σ_s MPa	M $hr^{-1}\times10^{-2}$	σ_t MPa	χ
SSM_T1	1.52	86.35	5.80	834.40	13
SSM_T2	3.83	87.58	6.90	834.40	13
SSM_T3	3.52	86.77	7.60	834.40	13

Table 5.3: Percentage of creep damage and instantaneous plastic damage in SSM at 650°C

Test ID	Creep Damage (%)	Instant Plastic Damage (%)
SSM_T1	71.34	28.66
SSM_T2	77.52	22.48
SSM_T3	82.36	17.64

CHAPTER 6: CONCLUSIONS AND FUTURE WORK

6.1 Conclusions

While new materials are developed for power generation, a need to characterize the creep properties of these materials in a short amount of time is necessary. A new self-calibration is vetted as another alternative to the current reference calibration approach seen applied in the TTSP/TSSP and SIM/SSM tests. The self-calibration approach presented in this thesis uses both the Theta Projection model and Sinh models to generate a master curve of creep data using an accelerated test.

Theta Projection Conclusions

- The percentage of time used to match the strain rates at the beginning and end of each stress step is the determinant for predicting creep rupture.
- While the equation is able to model primary and tertiary creep, the secondary creep regime is not accurately represented which in turn leads to over or under predictions of creep rupture
- The Theta Projection model cannot accurately predict creep rupture from accelerated creep testing

Sinh Conclusions

- The twofold calibration exercise reveals that determined material constants (λ, ϕ) are susceptible to stress variation. A strong stress dependency is observed in MCSR (λ) and SR (ϕ) related material constant.
- The sudden stepped increase in loading induce plastic damage into the test specimen instantaneously. This plastic damage accounts for one-fifth of the lifetime of the specimen.

The induced plastic damage coupled with creep damage lead the specimen to quick rupture, shortening the test duration. Though the specimen is subjected to plastic damage, the fidelity of the calibrated material constant by Sinh remain intact. Besides, Sinh model damage prediction accounts for the plastic damage in the damage trajectory.

- The Sinh can predict the SSM data with a high level of accuracy. The damage prediction evolves from zero to unity at rupture.
- The extrapolation credibility of Sinh is revealed the model's capability of extrapolating creep data up to 9.5 times the duration of test. The goodness of fit between extrapolated CCTs and experimental CCTs can be satisfactory for comparisons among candidate materials.
- The calibration approach resorted to in this paper assumes the model constants remain unaffected by instantaneous plastic damage, boundary condition change (stress variation), and micro-structural degradation. As creep mechanism is a complex process for metallic materials and superalloys and function of temperature and stress, the Micro-structural degradation and boundary condition variability could potentially influence the model constants. In a future study, effects of these aspect on the material constants and model performance will be investigated.

6.2 Future Work

Below are suggestions that not only can help improve these current experiments but allow for ease when developing new test matrices.

- Repeats of SSM and CCT experiments must be done to obtain similar microstructure, ensuring that deformation mechanism maps for the material that is being tested are gathered. This is to make sure that the material remains in one regime.

- Ensuring specimens are not tested within the plastic regime. The material constants of the Sinh model are affected by stress. Not only will this greatly improve the fits of the Sinh model but allow the material to have a similar microstructure as well.
- Conduct SSM and CCT experiments on other metals. As mentioned before, SSM and SIM are new approaches in metallics, so running experiments on other metals will further validate the approach of ACT.
- Investigate CALPHAD approach for development of new materials. This will allow material scientist to optimize mechanical properties and determine what phases will occur as new materials are developed for creep testing.
- Conduct SIM approach and compare results to SSM. This paper only focuses on the stepped isostress method, but testing is required for the stepped isothermal method. This will also validate if a constitutive model can be applied to different accelerated creep testing.

REFERENCES

[1] Stein-Brzozowska, G., Flórez, D. M., Maier, J., & Scheffknecht, G. (2013). Nickel-base superalloys for ultra-supercritical coal-fired power plants: Fireside corrosion. Laboratory studies and power plant exposures. Fuel, 108, 521-533.

[2] Reed, R. (2006). The Superalloys: Fundamentals and Applications. Cambridge: Cambridge University Press. doi:10.1017/CBO9780511541285

[3] Murty, K. L., & Charit, I. (2008). Structural materials for Gen-IV nuclear reactors: Challenges and opportunities. Journal of Nuclear Materials, 383(1-2), 189-195.

[4] Kimura, M., Kobayashi, K., & Yamaguchi, K. (2003). Creep and fatigue properties of newly developed ferritic heat-resisting steels for ultra super critical (USC) power plants. Journal of the Society of Materials Science, Japan, 52(3Appendix), 50-54.

[5] Betten, J., 2002, Creep Mechanics, Springer.

[6] Betten, J. (2008). Creep mechanics. Springer Science & Business Media.

[7] Kraus, H. (1980). Creep analysis. Research supported by the Welding Research Council. New York, Wiley-Interscience, 1980. 263 p.

[8] Mandziej, S. T. (2010). Simulative accelerated creep test on Gleeble. In Materials Science Forum (Vol. 638, pp. 2646-2651). Trans Tech Publications Ltd.

[9] Achereiner, F., Engelsing, K., Bastian, M., & Heidemeyer, P. (2013). Accelerated creep testing of polymers using the stepped isothermal method. Polymer Testing, 32(3), 447-454.

[10] Alwis, K. G. N. C., & Burgoyne, C. J. (2008). Accelerated creep testing for aramid fibres using the stepped isothermal method. Journal of materials science, 43(14), 4789-4800.

[11] Nobakhti, H., & Soltani, N. (2016). Evaluating small punch test as accelerated creep test using Larson–Miller parameter. Experimental Techniques, 40(2), 645-650.

[12] Bueno, B. D. S., Costanzi, M. A., & Zornberg, J. G. (2005). Conventional and accelerated creep tests on nonwoven needle-punched geotextiles. Geosynthetics International, 12(6), 276-287.

[13] Jeon, H. Y., Kim, S. H., & Yoo, H. K. (2002). Assessment of long-term performances of polyester geogrids by accelerated creep test. Polymer testing, 21(5), 489-495.

[14] Izaki, T., Kobayashi, T., Kusumoto, J., & Kanaya, A. (2009). A creep life assessment method for boiler pipes using small punch creep test. International Journal of Pressure Vessels and Piping, 86(9), 637-642.

[15] Nobakhti, H., & Soltani, N. (2016). Evaluating small punch test as accelerated creep test using Larson–Miller parameter. Experimental Techniques, 40(2), 645-650.

[16] Saucedo-Munoz, M. L., Komazaki, S. I., Takahashi, T., Hashida, T., & Shoji, T. (2002). Creep property measurement of service-exposed SUS 316 austenitic stainless steel by the small-punch creep-testing technique. Journal of materials research, 17(8), 1945-1953.

[17] Rouse, J. P., Cortellino, F., Sun, W., Hyde, T. H., & Shingledecker, J. (2013). Small punch creep testing: review on modelling and data interpretation. Materials Science and Technology, 29(11), 1328-1345.

[18] Barba, D., Reed, R. C., & Alabort, E. (2019). Ultrafast miniaturised assessment of high-temperature creep properties of metals. Materials Letters, 240, 287-290.

[19] Luo, W. B., Wang, C. H., & Zhao, R. G. (2007). Application of time-temperature-stress superposition principle to nonlinear creep of poly (methyl methacrylate). In Key engineering materials (Vol. 340, pp. 1091-1096). Trans Tech Publications.

[20] Schoeberle, B., Wendlandt, M., & Hierold, C. (2008). Long-term creep behavior of SU-8 membranes: Application of the time–stress superposition principle to determine the master creep compliance curve. Sensors and Actuators A: Physical, 142(1), 242-249.

[21] Giannopoulos, I. P., & Burgoyne, C. J. (2009, July). Stepped isostress method for aramid fibres. In 9th International Conference on Fiber Reinforced Polymers for Reinforced Concrete Structures (FRPRCS-9), Sydney, Australia.

[22] Giannopoulos, I. P., & Burgoyne, C. J. (2009). Stress limits for aramid fibres. Proceedings of the Institution of Civil Engineers-Structures and Buildings, 162(4), 221-232.

[23] Giannopoulos, I. P., & Burgoyne, C. J. (2011). Prediction of the long-term behaviour of high modulus fibres using the stepped isostress method (SSM). Journal of materials science, 46(24), 7660.

[24] Giannopoulos, I. P., & Burgoyne, C. J. (2012). Accelerated and real-time creep and creep-rupture results for aramid fibers. Journal of applied polyme science, 125(5), 3856-3870.

[25] Giannopoulos, I. P., & Burgoyne, C. J. (2009). Viscoelasticity of Kevlar 49 fibres. In 16th National Conference on Concrete Structures, Pafos, Cyprus.

[26] Tajvidi, M., Falk, R. H., & Hermanson, J. C. (2005). Time–temperature superposition principle applied to a kenaf-fiber/high-density polyethylene composite. Journal of applied polymer science, 97(5), 1995-2004.

[27] Vaidyanathan, T. K., Vaidyanathan, J., & Cherian, Z. (2003). Extended creep behavior of dental composites using time–temperature superposition principle. Dental Materials, 19(1), 46-53.

[28] Zornberg, J. G., Byler, B. R., & Knudsen, J. W. (2004). Creep of geotextiles using time–temperature superposition methods. Journal of geotechnical and geoenvironmental engineering, 130(11), 1158-1168.

[29] Hadid, M., Guerira, B., Bahri, M., & Zouani, A. (2014). Assessment of the stepped isostress method in the prediction of long term creep of thermoplastics. Polymer Testing, 34, 113-119.

[30] Zornberg, J. G., Byler, B. R., & Knudsen, J. W. (2004). Creep of geotextiles using time–temperature superposition methods. Journal of geotechnical and geoenvironmental engineering, 130(11), 1158-1168.

[31] Evans, R. W., & Wilshire, B. (1985). Creep of metals and alloys.

[32] Brown, S. G. R., Evans, R. W., & Wilshire, B. (1986). A comparison of extrapolation techniques for long-term creep strain and creep life prediction based on equations designed to represent creep curve shape. International Journal of Pressure Vessels and Piping, 24(3), 251-268.

[33] Brown, S. G. R., Evans, R. W., & Wilshire, B. (1986). Creep strain and creep life prediction for the cast nickel-based superalloy IN-100. Materials Science and Engineering, 84, 147-156.

[34] Evans, R. W., Parker, J. D., & Wilshire, B. (1992). The θ projection concept—A model-based approach to design and life extension of engineering plant. International Journal of Pressure vessels and piping, 50(1-3), 147-160.

[35] Stewart, C. M., 2013, "A Hybrid Constitutive Model for Creep, Fatigue, and Creep-Fatigue Damage," University of Central Florida.

[36] Haque, M. S., 2015, "An Improved Sin-Hyperbolic Constitutive Model for Creep Deformation and Damage," The University of Texas at El Paso.

[37] Haque, M. S., and Stewart, C. M., 2016, "Finite-Element Analysis of Waspaloy Using Sinh Creep-Damage Constitutive Model Under Triaxial Stress State," J. Press. Vessel Technol. Trans. ASME, 138(3), pp. 1–9.

[38] Haque, M. S., and Stewart, C. M., 2016, "Exploiting Functional Relationships Between MPC Omega, Theta, and Sine-Hyperbolic Continuum Damage Mechanics Model," *Proceedings of ASME 2016 Pressure Vessels and Piping Conference PVP 2016*, Vancouver, British Columbia, Canada, pp. 1–11.

[39] Campbell, F., 2008. Elements Of Metallurgy And Engineering Alloys. Materials Park, Ohio: ASM International.

[40] Vander Voort, G., & Manilova, E. (2004). Metallographic techniques for superalloys. Microscopy and Microanalysis, 10(S02), 690-691.

[41] Standard Test Method for Tension Testing of Metallic Materials, August (2013), DOI: 10.1520/E0008_E0008M-13A

[42] American Society of Testing and Methods, 2015 "ASTM Standard E139 Test Method for Conducting Creep, Creep-Rupture, and Stress-Rupture Tests of Metallic Materials," ASTM International, West Conshohocken, PA.

[43] UNS N07718, (2018), "Special Metals – Inconel 718 alloy," U.S.A. Special Metals Corporation, 3200 Riversie Drive, Huntington, WV, www.specialmetals.com.

[44] American Society of Testing and Methods, “ASTM Standard E21 Standard Test Methods for Elevated Temperature Tension Test of Metallic Materials,” ASTM International, West Conshohocken, PA, 2009.

[45] Harold J Frost and M. F. Ashby, 1982, Deformation-Mechanism Maps, The Plasticity and Creep of Metals and Ceramics, Pergamon Press, Oxford.

[46] Kim, W. G., Yin, S. N., Kim, Y. W., & Chang, J. H. (2008). Creep characterization of a Ni-based Hastelloy-X alloy by using theta projection method. Engineering Fracture Mechanics, 75(17), 4985-4995.

[47] ASTM International. (2016). D6992-16 Standard Test Method for Accelerated Tensile Creep and Creep-Rupture of Geosynthetic Materials Based on Time-Temperature Superposition Using the Stepped Isothermal Method. Retrieved from https://doi.org/10.1520/D6992-16

VITA

My name is Robert Mach. I graduated with my Bachelor of Science from the University of Texas at El Paso (UTEP) in December of 2018. This thesis is submitted as a requirement for the completion of a master's degree in Mechanical Engineering at UTEP as well under the supervision of Dr. Calvin M. Stewart. The current work is a compilation of the work I have done as a research assistant in the Materials at Extremes Research Group (MERG). With MERG, I have studied various materials since I was an undergraduate, from polymer bonded explosives, to asphalts, to nickel-based superalloys. The topics I have learned from my research experience include, fracture mechanics, failure analysis, creep damage, creep deformation, as well as some modeling.

The publications related to this work include

1) Mach, R., Pellicotte, J., Haynes, A., & Stewart, C. (2019, June). Assessment of Long Term Creep Using Strain Rate Matching From the Stepped Isostress Method. In Turbo Expo: Power for Land, Sea, and Air (Vol. 58684, p. V07AT31A011). American Society of Mechanical Engineers.
2) Hossain,A., Mach, R., & Stewart, C. (2020, June). Calibration of CDM-Based Creep Constitutive Model Using Accelerated Creep Test (ACT) Data. In Turbo Expo. American Society of Mechanical Engineers. (Paper accepted)
3) Stewart, C., Hossain,A., Mach, R., & Pellicotte, J., & (2020). "Accelerated Creep Testing of Inconel 718 using the Stepped Isostress Method (SSM)" (Manuscript in preparation)

Contact information: Robert Mach, institute email: rmmach@miners.utep.edu, personal email: robmach96@outlook.com